Solid Solution Phases in the Olivine-Type $LiMnPO_4/MnPO_4$ System

Guoying Chen* and Thomas J. Richardson*, z

Environmental Energy Technologies Division

Lawrence Berkeley National Laboratory

Berkeley, California 94720 USA

Abstract

Nonstoichiometry is reported in the $LiMnPO_4/MnPO_4$ system for the first time. As lithium is removed from crystalline $LiMnPO_4$ by chemical or electrochemical methods, the resulting two phase mixture consists of stoichiometric $LiMnPO_4$ and a delithiated phase, Li_yMnPO_4, whose lattice parameters depend upon the global extent of delithiation and on the crystalline domain size of the delithiated phase. This behavior is reproduced during electrochemical insertion of lithium. Again, no evidence for nonstoichiometry was found in the vicinity of $LiMnPO_4$. Attempts to create single phase solid solutions by heating mixtures of the two phases failed due to the thermal instability of Li_yMnPO_4.

* Electrochemical Society Active Member

z E-mail: tjrichardson@lbl.gov

Introduction

For the last two decades, Olivine-type $LiMPO_4$ (M = Fe, Mn, Co and Ni) have been attractive cathode materials for lithium-ion batteries owing to their stability and low cost. [1] One of the development challenges lies in understanding and controlling the phase transition processes in which Li is extracted from or inserted into the phosphates. After years of discussion and debates, the facile two-phase reaction between $LiFePO_4$ and $FePO_4$ remains a puzzle, as neither of the end members possesses the high electronic and/or ionic conductivities that are usually characteristic of materials capable of fast phase transformation. A popular explanation involves the formation of more conductive solid solutions, $Li_\alpha FePO_4$ and $Li_{1-\beta}FePO_4$ (α and β are close to 0), during the transition. Models based on solid solutions were developed by Srinivasan et al., [2-3] and experimental observation of room temperature non-stoichiometric phases was first reported by Yamada et al. through chemical oxidation/reduction, X-ray diffraction studies, calorimetric measurements and neutron diffraction studies. [4-5] The electrochemical properties and the relevance of room temperature solid solution phases to the mechanism of the phase transition(s), however, are still not clear. Li_xFePO_4 solid solutions do exist for all values of x at elevated temperatures. [6-10]

Recently, the effect of particle size on the formation of room temperature solid solutions has been emphasized. Yamada et al [5, 11] reported the variation of α and β in $Li_\alpha FePO_4$ and $Li_{1-\beta}FePO_4$ phases with particle size, and suggested that their formation is kinetically hindered in large particles (> 900 nm). Chiang et al. [12-14] showed that the room temperature miscibility gap is controlled by particle size, and claimed that the gap disappears altogether in particles smaller than 15 nm. This was supported by the

experimental work from Gibot et al., [15] who recently reported a single-phase Li extraction/insertion process in a 40 nm $LiFePO_4$ sample.

For $LiCoPO_4$ and $LiNiPO_4$, the studies are scarce because of electrolyte instability in the high voltage range of these materials. Nakayama et al. showed the existence of two plateaus exist during electrochemical charging of $LiCoPO_4$. [16] In contrast to $LiFePO_4$, a three-phase system was proposed, with delithiation proceeding *via* the formation of an intermediate phase, Li_zCoPO_4 (z was initially determined to be 0.70 and recently modified to 0.60). [17-19] The intermediate subsequently transforms to $CoPO_4$, which has low stability at room temperature and rapidly becomes amorphous.

Although it has been assumed that the phase transition in $LiMnPO_4$ is similar to that of $LiFePO_4$, namely a two-phase process involving $LiMnPO_4$ and $MnPO_4$ with the possibility of some nonstoichiometry in the end members, a detailed mechanism has not been put forward. Here we have investigated the phase transformation in hydrothermally synthesized $LiMnPO_4$ crystals, and report observation of Li_yMnPO_4 room temperature solid solutions for the first time. Throughout this paper, we use x to denote the fraction of $LiMnPO_4$ in the sample, and y the amount of lithium present in the delithiated phase.

Experimental

Synthesis

$LiMnPO_4$ crystals were synthesized as described previously. [20] $MnSO_4.H_2O$ (Mallinckrodt, Inc) or $Mn(NO_3)_2.4H_2O$ (Aldrich) was mixed with an equimolar amount of H_3PO_4 (85%, J. T. Baker) in deionized and deoxygenated water. A 1.5 M LiOH (Spectrum) solution was added slowly with stirring to give Mn:P:Li equal to 1:1:3.

Substantial precipitation occurred during this step. After stirring under helium for another 5 min, the reaction mixture was transferred to a 125 ml Teflon-lined reactor, which was sealed after purging with helium, then held at 220 °C for 5 h. On cooling to room temperature, the off-white precipitate was filtered, thoroughly washed with deionized water, and dried in a vacuum oven at 60 °C for 24 h.

Varying degrees of chemical delithiation were achieved by stirring $LiMnPO_4$ samples in aliquots of a 0.1 M solution of nitronium tetrafluoroborate (NO_2BF_4, 95+%, Aldrich) in acetonitrile for 24 h. The reactions were carried out at room temperature in an argon-filled glovebox with $O_2 < 1$ ppm and $H_2O < 2$ ppm.

Electrochemical studies

$LiMnPO_4$ crystals prepared from the nitrate precursor were ball milled with 20 wt% acetylene carbon black for 30 min. Composite electrodes were prepared by mixing 80 wt% of this mixture, 10 wt% of Kynar 2801 poly(vinylidene fluoride) (PVdF) binder (Elf Atochem North America, Inc.), 5 wt% SFG-6 synthetic flake graphite (Timcal Ltd., Graphites and Technologies), and 5 wt% compressed acetylene black in *N*-methylpyrrolidone (NMP) solution. The slurry was spread onto carbon-coated aluminum foil current collectors and dried overnight in air and then in a 120 °C vacuum oven for 10 h. Electrodes (4.0 cm x 2.0 cm) were mounted in a single compartment three-electrode cell, with Li foil as reference and counter electrodes, and 1 M $LiPF_6$ in 1:1 propylene carbonate (PC):ethylene carbonate electrolyte (EC). Lithium was extracted potentiostatically at 4.5 V to a preselected state of charge (SOC). At each SOC, the electrode was removed from the cell, washed free of electrolyte with dimethyl carbonate

(DMC), and examined by XRD. Discharging of the electrode was carried out in the same manner at 2.5 V.

Characterization

X-ray diffraction (XRD) patterns were acquired using a Panalytical Xpert Pro diffractometer equipped with monochromatized Cu Kα radiation. The scan rate was 0.0025°/s in 0.01° steps for the powder samples, and 0.001°/s in 0.01° steps for the electrodes. Lattice parameters and phase ratios in the oxidized samples were determined by pattern refinement using Riqas software (Materials Data, Inc.). Thermogravimetric analysis (TGA) was carried out on a simultaneous thermal analyzer (STA 449 F3, NETZSCH) under Ar atmosphere, with a heating rate of 10 °C/min. Scanning electron microscopy (SEM) images were collected using a Hitachi S-4300 SE/N microscope at 20 kV accelerating voltage. Fourier transform infrared spectroscopy (FTIR) measurements were performed on KBr pellets using a Nicolet 6700 spectrometer in transmission mode with a spectral resolution of 4 cm^{-1}.

Results and Discussion

Formation of Li_yMnPO_4 solid solutions during chemical oxidation

The size and shape of hydrothermally synthesized crystals are largely controlled by reaction conditions. [21] Fig. 1 shows the SEM images of three $LiMnPO_4$ samples that were prepared with different Mn^{2+} concentrations or Mn^{2+} precursor. Both samples A and B were synthesized from $MnSO_4$ precursor, with the Mn^{2+} concentration in the latter case at 0.3 M, 5 times higher than that in sample A. The particles were diamond-shaped

aggregates composed of small crystals, and they measured about 8 um and 2 um respectively in the long axis. When $Mn(NO_3)_2$ was used as Mn^{2+} source instead of $MnSO_4$ (Sample C), the morphology of the $LiMnPO_4$ crystals was quite different. They consisted of discrete, elongated hexagonal plates measuring about 0.6 μm x 0.4 μm x 0.1 μm. Selected area electron diffraction (SAED) showed that these dimensions correspond to the *c*, *a*, and *b*-axes, respectively. The difference on morphology may be due to the change in initial pH, which decreased from 10.5 to 9 when using the nitrate precursor. Alternatively, the solubility of precipitates may be affected.

Chemical delithiation of $LiMnPO_4$ can be achieved by reaction with NO_2BF_4, an oxidant with a potential of *ca.* 5.1 V *vs.* Li/Li^+. [22-23] Fig. 2 compares the XRD patterns of samples A, B and C after treatment with a twofold excess of NO_2BF_4 for 24 h. Under these conditions, a larger amount of the delithiated phase was formed in Sample C, which had a smaller secondary particle size, even though samples A and B were aggregates with crystalline domain size of 28 nm vs. 45 nm for sample C. Full pattern XRD refinements showed levels of 60%, 70% and 100% of this phase in the oxidized A, B, and C samples. The crystalline domain size of the phase increased along with amount, reaching 6, 10 and 16 nm, respectively. The unit cell volume, on the other hand, decreased from 279.9 $Å^3$ in sample A, to 276.8 in sample B, and 272.5 $Å^3$ in sample C.

In large, aggregated crystals, the oxidation was not complete after 24 hr, even with the excess of oxidant. The domains of the newly formed phase were smaller, and the cell dimensions indicated that it was a Li_yMnPO_4 solid solution rather than the fully delithiated $MnPO_4$. The Li content, *y*, decreased with the particle size of the sample. This may explain the large variation in lattice parameters of $MnPO_4$ that are reported in the

literature. The documented unit cell volumes range from 269.6 to 275.0 $Å^3$ in studies carried out on a variety of $LiMnPO_4$ samples by several groups. [13, 22, 24-25]

Room temperature delithiation was further investigated by treating $LiMnPO_4$ crystals (Sample C) with varying amounts of NO_2BF_4 for 24 h. The amount of the delithiated phase produced increased monotonically with the amount of oxidant used. The reaction under these conditions, however, was not stoichiometric, as only 30% delithiation was achieved for a 1:1 molar ratio of NO_2BF_4. Extending the reaction time improved the yield, but complete oxidation was not achieved even after 3 days. The delithiated phase grew much faster with an excess of NO_2BF_4, as shown by the increased slope in the region of over 100% oxidant (Fig. 3).

Fig. 4 shows the *ex-situ* XRD patterns of these samples at different levels of oxidation. As lithium extraction proceeded, the relative amount of the delithiated phase increased, while the peaks due to the delithiated phase shifted in position. As is clearly seen in the 211/020 region, the Li_yMnPO_4 peak gradually moved towards higher angle as the lithium content in the sample decreased. Refinement established the lattice dimensions, crystalline domain sizes and the amount of each phase in the oxidized mixtures. Fig. 5a shows the lattice parameters for the delithiated phase. As the amount of this phase in the sample increased, *a*, *b* and the unit cell volume decreased while lattice parameter *c* increased slightly. This reflects a gradual removal of Li and the formation of Li_yMnPO_4 solid solution. The changes for cell parameters *a, b,* and *V* were -0.5%, -1.3% and -1.8%, respectively, when the fraction of the lithiated phase *x* decreased from 0.93 to 0. Assuming the phase formed at $x = 0$ is fully delithiated and that Vegard's law applies in the system, the residual Li (y) when $x = 0.93$ had its highest observed value of 0.16.

The cell parameters changed more rapidly in the region where $x > 0.70$, and they stabilized at x close to 0.30.

Fig. 5b shows the unit cell volume and crystalline domain size of the delithiated phase as functions of its fraction in the sample. As before, the crystalline domain size increased steadily with the mole fraction, reaching 16 nm when the sample was fully oxidized. There was a steady decrease in unit cell volume with increasing domain size, from 277.5 $Å^3$ at 2 nm to 272.5 $Å^3$ at 16 nm. These results demonstrate that the residual Li in the delithiated phase is closely related to its domain size. A higher concentration of Li can remain in domains that are smaller than 10 nm, decreasing significantly as the domains grow to above 10 nm. Although the domain size of the lithiated phase decreased from 45 nm to 18 nm when x changed from 1.0 to 0.20, the cell dimensions remained essentially constant across the entire SOC range (Fig. 5c), reflecting the absence of Li non-stoichiometry in this phase.

A similar trend was found in the FTIR spectra (Fig 6) of the oxidized samples and end members. As the Li content decreased, the intensity of the peaks due to $LiMnPO_4$ decreased and those of the delithiated phase increased. In the low frequency region, the peak at 632 cm^{-1} arises from the lithiated phase, while the peak between 650 cm^{-1} to 660 cm^{-1} originates from the delithiated phase (Fig 6a). In the latter case, there was a gradual shift towards higher frequency as the amount of the delithiated phase in the sample increased (Fig 6b), reflecting a decrease in Li concentration in the phase. The change was again more rapid as oxidation began, and it leveled off when there was about 70% of the delithiated phase (x=0.30) in the mixture. This is consistent with the XRD observations, and provides additional support for the existence of Li_yMnPO_4 solid

solutions. No changes were observed in the peak positions of the lithiated phase. At this point, it is difficult to say that the delithiated phase in the fully oxidized sample is truly $MnPO_4$, as there is no consistent literature data for comparison. More experiments that allow nucleation and growth of $MnPO_4$ domains into larger size, such as oxidation of $LiMnPO_4$ at a somewhat higher temperature, may help to answer this question.

Formation of Li_yMnPO_4 solid solutions during electrochemical charging and discharging

The formation of Li_yMnPO_4 solid solutions was also observed when $LiMnPO_4$ crystals (Sample C) were electrochemically charged and discharged. A composite electrode was charged to give lithium contents of 0.64, 0.52, 0.22 and 0.14, as determined by coulometer. Complete extraction of Li was not achieved even at 4.5 V due to the high resistance of the electrode. Fig. 7a shows the *ex-situ* XRD patterns in the 211/020 region at each SOC, with the pattern of the chemically delithiated phase (x = 0) added for comparison. The peak position of the delithiated phase gradually shifts as more lithium is extracted. The cell volume of the delithiated phase decreased from 278.4 $Å^3$ to 275.6 $Å^3$ as the global Li content x decreased from 0.64 to 0.14 (Fig 7b). The cell volume of the lithiated phase, on the other hand, remained constant.

The electrode that was previously charged to a lithium content of 0.14 was discharged in steps to 0.32, 0.68 and 0.85, further re-lithiation at 2.5 V was unsuccessful. *Ex-situ* XRD patterns in the 211/020 region at each SOC are shown in Fig 8a. Again a gradual peak shift of the delithiated phase was observed, and the unit cell volume of the phase increased from 275.6 $Å^3$ at a lithium content of 0.14 to 282.0 $Å^3$ at 0.85 (Fig 8b).

The cell dimension of the lithiated phase once again remained unchanged during the process.

The $LiMnPO_4$ crystals used in our study are sub-micron in size, but well above the range where room temperature Li_xFePO_4 solid solutions have been reported to exist. The results from these chemical and electrochemical studies indicate that Li_yMnPO_4 solid solutions near the end of charge can form and persist in relatively large particles, provided that the domain size of that phase is small. In contrast to the $LiFePO_4/FePO_4$ system, in which the stable delithiated end member nucleates and grows into large domains quickly, [26] the accumulation of elastic energy in small delithiated $LiMnPO_4$ domains restricts their growth and allows the accommodation of a significant concentration of residual Li in the phase. On the other hand, Li non-stoichiometry was not observed in the lithiated phase. Some hysteresis was observed during the phase transformation, as shown by the history-dependent unit cell volumes for similar states of charge. Fig. 9 compares the cell volumes of the chemically oxidized samples with those of the electrochemically charged and discharged electrodes. The cell volume reached its lowest value in the sample that was chemically oxidized, corresponding to the smallest amount of residual Li in the phase. The largest unit cell (and presumably the highest Li content) in a delithiated phase was observed in the sample that was electrochemically charged and then discharged. This is likely due to the smaller domain size of the phase formed during the electrochemical processes, as evidenced by broader peaks in their XRD patterns. Discharging the previously charged electrode divided the domains of the delithiated phase into even smaller sizes, which allowed for higher amounts of residual Li.

Solid solution behavior during thermal treatment

The thermal behavior of the olivine $LiFePO_4/FePO_4$ system has been well studied in recent years. It was shown that the miscibility gap between the two end members shrinks and single-phase solid solutions form when two-phase mixtures are heated to about 300 °C. [6-8] No similar studies have been reported on the $LiMnPO_4$ system. In an effort to prepare and characterize such single phase solid solutions, chemically delithiated ($xLiMnPO_4/(1-x)Li_yMnPO_4$) samples with $x = 0.70$ and 0 were heated under N_2 to 375 °C, and then cooled. Fig. 10 compares the XRD patterns of the cooled samples, along with the pattern from similarly treated $LiMnPO_4$. While $LiMnPO_4$ was unaffected, the delithiated phase decomposed to form $Mn_2P_2O_7$, characterized by strong diffraction peaks at 29° and 30.5°. In contrast to the behavior of $LiFePO_4/FePO_4$, single-phase solid solutions were not formed due to the instability of Li_yMnPO_4.

This decomposition was further investigated by thermogravimetric analysis (Fig 11). While $LiMnPO_4$ showed no weight change during heating to 600 °C in an argon atmosphere, both the single-phase delithiated sample ($x = 0$) and the $0.7LiMnPO_4/0.3Li_yMnPO_4$ mixture lost weight between 100 °C and 400 °C. The total weight losses (11% and 6%, respectively) were much larger than expected for O_2 evolution to form $M_2P_2O_7$ (5.4% and 1.6%). This is most likely due to absorption of water during transfer to the TGA crucible, as the delithiated phase is strongly hygroscopic and the sample size for the experiment is small. For comparison, the weight of a $0.77LiFePO_4/0.23FePO_4$ two-phase mixture was essentially constant up to 600 °C. Small particle size and hydrate formation may contribute to the near disappearance of the XRD peaks of the delithiated phase following prolonged chemical oxidation of $LiMnPO_4$,

as reported by Yamada and Chung[27] . The higher peak intensity observed here may relate to the use of $LiMnPO_4$ crystals with a primary particle size of hundreds rather than tens of nm. This leads to the formation of a delithiated phase with higher crystallinity and lower moisture sensitivity. A broad XRD peak near 26°, associated with hydration of the delithiated phase, was detected after oxidized samples were exposed to air for a long periods of time.

Conclusions

Li_yMnPO_4 solid solution phases with composition near to $MnPO_4$ are formed at room temperature during chemical delithiation and during both extraction and insertion of lithium electrochemically. There is a strong correlation between the global lithium content and residual lithium in the delithiated phase, as well as with the crystalline domain size of the latter. The lattice parameters of the solid solution phase approach those reported for $MnPO_4$ as the fraction of the remaining $LiMnPO_4$ decreases. Heating $x LiMnPO_4/(1-x)Li_yMnPO_4$ two-phase mixtures does not produce single-phase solid solutions due to decomposition of the delithiated phase. This study demonstrates fundamental differences between the $LiFePO_4$ and $LiMnPO_4$ systems, mostly as a consequence of increased lattice mismatching and lower stability in the latter system.

Acknowledgements

We thank James Wilcox for preparing the composite electrode. This work was supported by the Assistant Secretary for Energy Efficiency and Renewable Energy,

Office of FreedomCAR and Vehicle Technologies of the U. S. Department of Energy under Contract No. DE-AC02-05CH11231.

Table 1. Hydrothermally synthesized $LiMnPO_4$ samples

Sample	Mn^{2+} precursor	Mn^{2+} concentration	Particle morphology	Particle size (μm)	Primary Particle size (nm)
A	$MnSO_4$	0.06 M	diamond-shaped aggregates	8 x 2 x 1	200-800
B	$MnSO_4$	0.3 M	diamond-shaped aggregates	2 x 1 x 0.5	200
C	$Mn(NO_3)_2$	0.3 M	hexagonal plates	0.6 x 0.4 x 0.1	600

References

[1] A. K. Padhi, K.S. Nanjundaswamy, J.B. Goodenough, J. Electrochem. Soc., 144, 1188 (1997).

[2] V. Srinivasan and J. Newman, *J. Electrochem. Soc.*, **151**, A1517 (2004).

[3] V. Srinivasan and J. Newman, *Electrochem. Solid-State Lett.*, **9**, A110 (2006).

[4] A. Yamada, H. Koizumi, N. Sonoyama, and R. Kanno, *Electrochem. Solid-State Lett.*, **8**, A409 (2005).

[5] A. Yamada, H. Koizumi, S.-I. Nishimura, N. Sonoyama, R. Kanno, M. Yonemura, T. Nakamura, and Y. Kobayashi, *Nat. Mater.*, **5**, 357 (2006).

[6] C. Delacourt, P. Poizot, J.-M. Tarascon, and C. Masquelier, *Nat. Mater.*, **4**, 254 (2005).

[7] J. L. Dodd, R. Yazami, and B. Fultz, *Electrochem. Solid-State Lett.*, **9**, A151 (2006).

[8] G. Chen, X. Song, and T. J. Richardson, *J. Electrochem. Soc.*, **154**, A627 (2007).

[9] F. Zhou, T. Maxisch, and G. Ceder, *Phys. Rev. Lett.*, **97**, 155704 (2006).

[10] B. Ellis, L. K. Perry, D. H. Ryan, and L. F. Nazar, *J. Am. Chem. Soc.*, **128**, 11416 (2006).

[11] G. Kobayashi, S.-I. Nishimura, M.-S. Park, R. Kanno, M. Yashima, T. Ida, and A. Yamada, *Adv. Funct. Mater.*, **19**, 395 (2009).

[12] N. Meethong, H.-Y. S. Huang, W. C. Carter, and Y.-M. Chiang, *Electrochem. Solid-State Lett.*, **10**, A134 (2007).

[13] N. Meethong, H.-Y. S. Huang, S. A. Speakman, W. C. Carter, and Y.-M. Chiang, *Adv. Funct. Mater.*, **17**, 1115 (2007).

[14] N. Meethong, Y.-H. Kao, M. Tang, H.-Y. Huang, W. C. Carter, and Y.-M. Chiang, *Chem. Mater*, **20**, 6189 (2008).

[15] P. Gibot, M. Casas-Cabanas, L. Laffont, S. Levasseur, P. Carlach, S. hamelet, J.-M. Tarascon, and C. Masquelier, *Nat. Mater.*, **7**, 1 (2008).

[16] M. Nakayama, S. Goto, Y. Uchimoto, M. Wakihara, and Y. Kitajima, *Chem. Mater.*, **16**, 3399 (2004).

[17] N. N. Bramnik, K. Nikolowski, C. Baehtz, K. G. Bramnik, and H. Ehrenberg, *Chem. Mater.*, **19**, 908 (2007).

[18] N. N. Bramnik, K. Nikolowski, D. M. Trots, and H. Ehrenberg, *Electrochem. Solid-State Lett.*, **11**, A89 (2008).

[19] H. Ehrenberg, N. N. Bramnik, A. Senyshyn, and H. Fuess, *Solid State Sci.*, **11**, 18 (2009).

[20] G. Chen, X. Song, and T. J. Richardson, *Electrochem. Solid-State Lett.*, **9**, A295 (2006).

[21] B. Ellis, W. H. Kan, W. R. M. Makahnouk, and L. F. Nazar, *J. Mater. Chem.*, **17**, 3248 (2007).

[22] C. Delacourt, L. Laffont, R. Bouchet, C. Wurm, J.-B. Leriche, M. Morcrette, J.-M. Tarascon, and C. Masquelier, *J. Electrochem. Soc.*, **152**, A913 (2005).

[23] G. Chen, X. Song, and T. J. Richardson, *Electrochem. Solid-State Lett.*, **11**, A190 (2008).

[24] G. Li, H. Azuma, and M. Tohda, *Electrochem. Solid-State Lett.*, **5**, A135 (2002).

[25] C. Delacourt, P. Poizot, J.-M. Tarascon, and C. Masquelier, *Chem. Mater.*, **16**, 93 (2004).

[26] C. Delmas, M. Maccario, L. Croguennec, F. Le Cras, and F. Weill, *Nat. Mater.*, **7**, 665 (2008).

[27] A. Yamada and S.-C. Chung, *J. Electrochem. Soc.*, **148**, A960 (2001).

Figure captions

1. SEM images of $LiMnPO_4$ samples prepared from a) a 0.06 M $MnSO_4$ precursor, b) a 0.3 M $MnSO_4$ precursor, and c) a 0.3 M $Mn(NO_3)_2$ precursor.
2. XRD patterns of $LiMnPO_4$ samples oxidized by a twofold excess of NO_2BF_4. Insert: variation in 211/020 peak intensities.
3. Efficiency of the NO_2BF_4 oxidation reaction.
4. XRD patterns of the xLiMnPO$_4$/(1-x)Li$_y$MnPO$_4$ samples. Insert: variation in 211/020 peak intensities.
5. a) Lattice parameters and unit cell volumes of the delithiated phase in the xLiMnPO$_4$/(1-x)Li$_y$MnPO$_4$ two-phase mixtures, and the relationship between the domain size, mole fraction and the unit cell volume of the delithiated phase b) and the lithiated phase c).
6. a) FTIR spectra of xLiMnPO$_4$/(1-x)Li$_y$MnPO$_4$ samples in the low frequency range; b) the relationship between the peak position and oxidation state of the sample.
7. a) *Ex-situ* XRD patterns of a Li$_x$MnPO$_4$ electrode at various stages of electrochemical extraction of lithium; b) the relationship between the unit cell volumes of the phases and the charge state of the sample.
8. a) *Ex-situ* XRD patterns of a Li$_x$MnPO$_4$ electrode at various stages of electrochemical insertion of lithium; b) the relationship between the unit cell volumes of the phases and the discharge state of the sample.
9. Comparison of the relationships between the unit cell volumes and oxidation states of samples from chemical and electrochemical testing.

10. XRD patterns of a) cooled Li_yMnPO_4, b) cooled $0.7LiMnPO_4/0.3Li_yMnPO_4$, c) $0.7LiMnPO_4/0.3Li_yMnPO_4$ two phase mixture before heating, and d) cooled $LiMnPO_4$. Insert: variation in 211/020 peak intensities. Lines indicate the peaks from $Mn_2P_2O_7$.
11. Thermogravimetric analysis of a) $LiMnPO_4$, b) $0.77LiFePO_4/0.23FePO_4$ two-phase mixture, c) $0.7LiMnPO_4/0.3Li_yMnPO_4$ two-phase mixture, and d) Li_yMnPO_4.

Figure 1

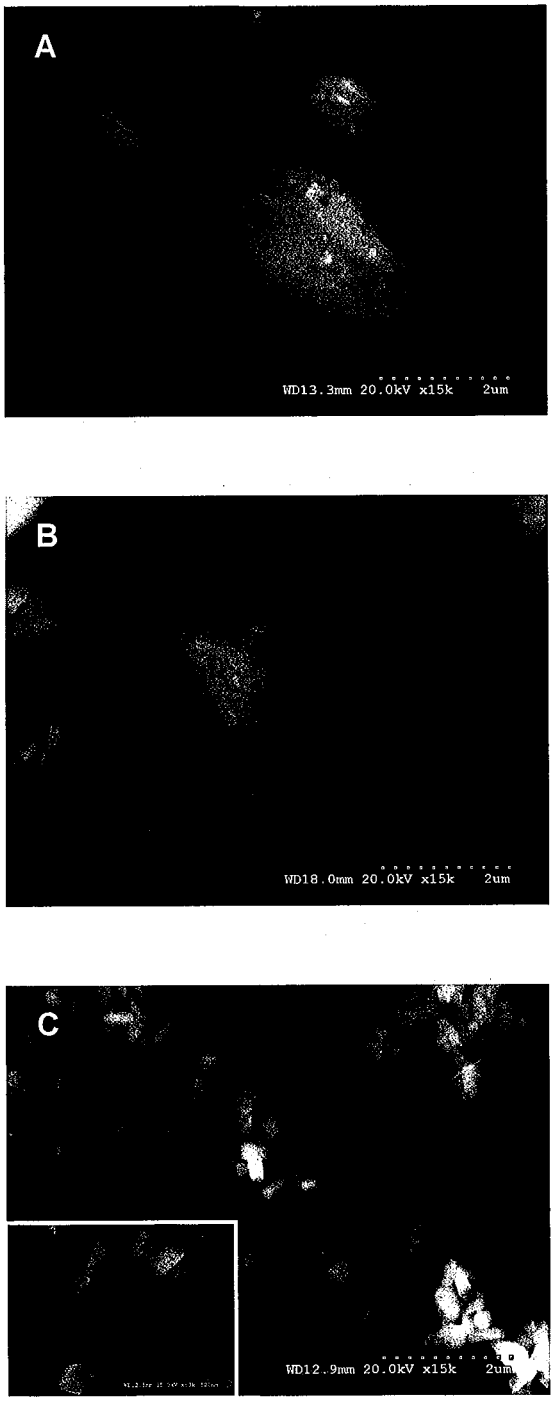
A
WD13.3mm 20.0kV x15k 2um
B
WD18.0mm 20.0kV x15k 2um
C
WD12.9mm 20.0kV x15k 2um

Figure 2

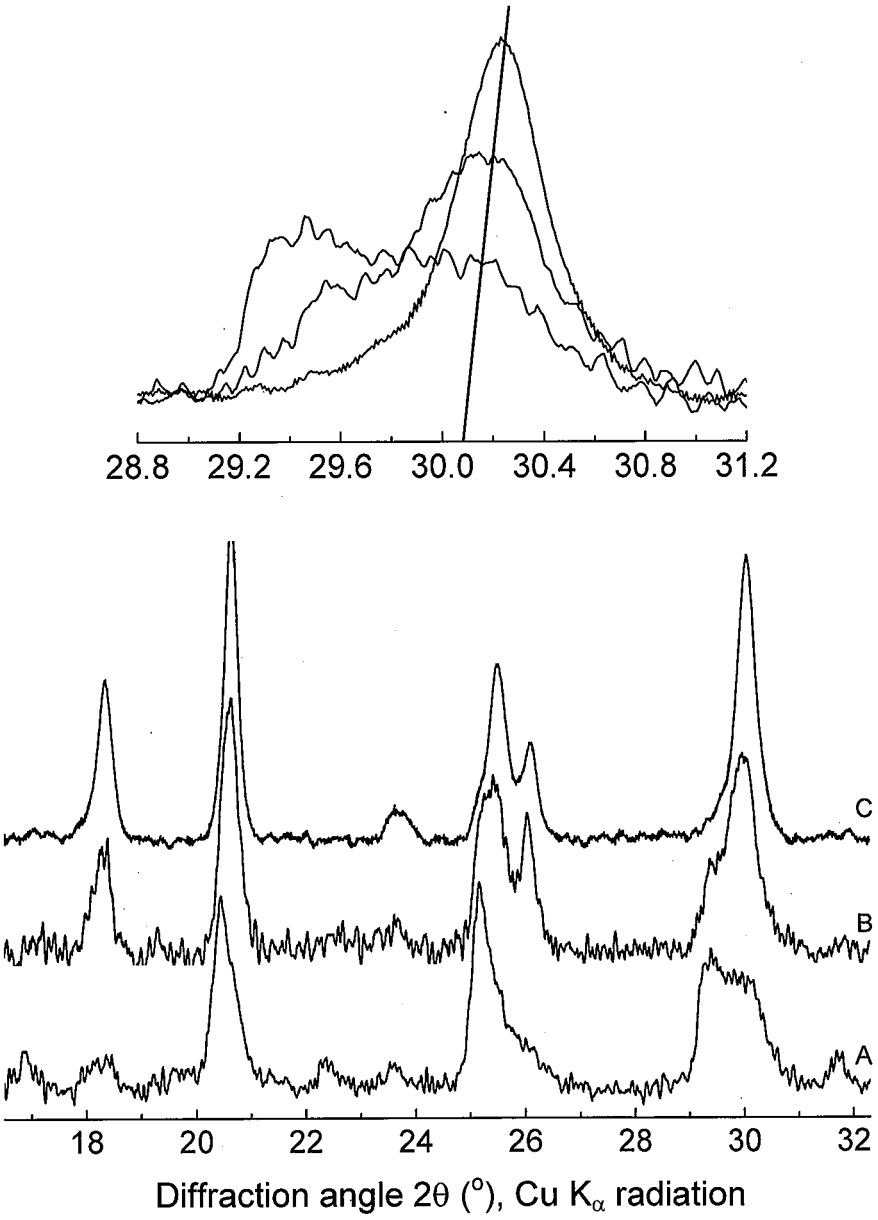
28.8
29.2
29.6
30.0
30.4
30.8
31.2
C
B
A
18
20
22
24
26
28
30
32
Diffraction angle 2θ (°), Cu Kα radiation

Figure 3

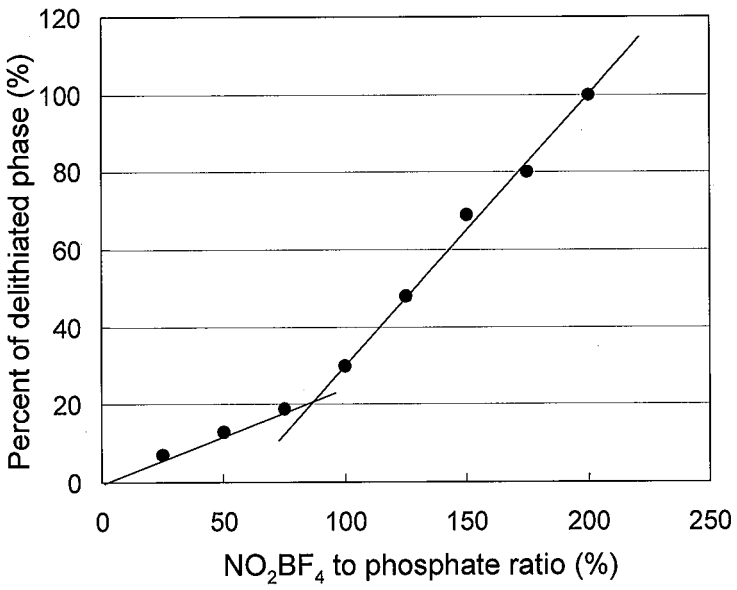
120
100
80
60
40
20
0
Percent of delithiated phase (%)
0
50
100
150
200
250
NO_2BF_4 to phosphate ratio (%)

Figure 4

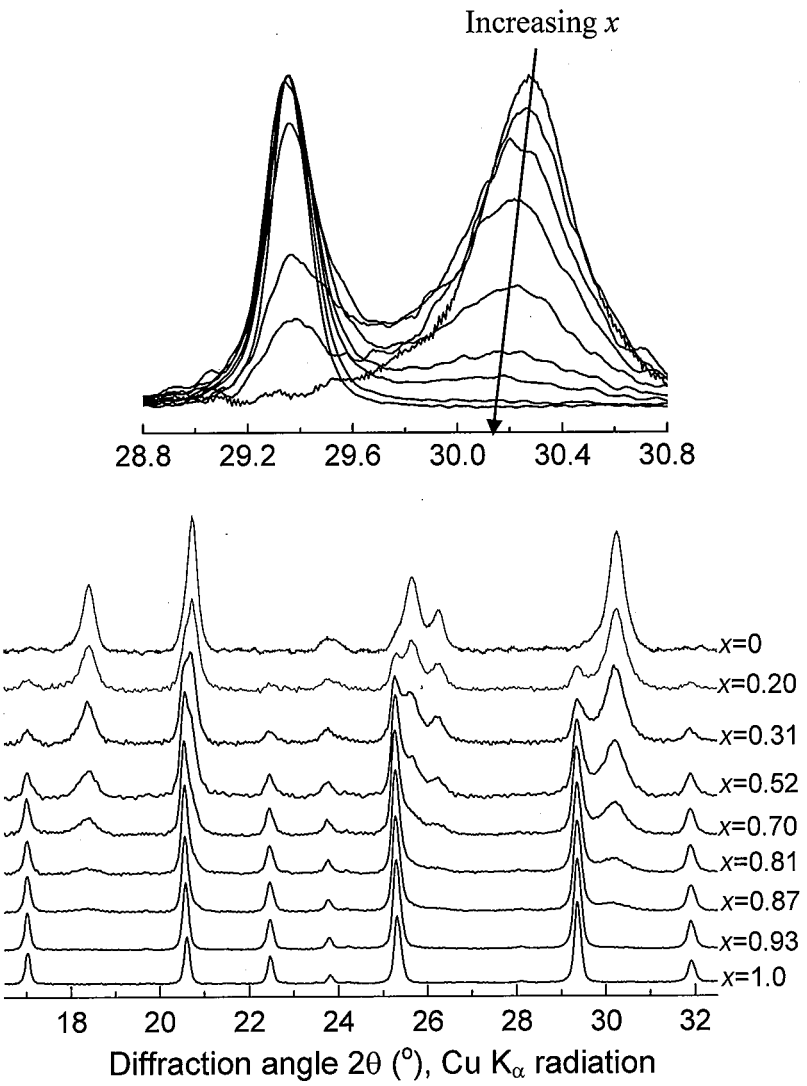
Increasing x
28.8
29.2
29.6
30.0
30.4
30.8
x=0
x=0.20
x=0.31
x=0.52
x=0.70
x=0.81
x=0.87
x=0.93
x=1.0
18
20
22
24
26
28
30
32
Diffraction angle 2θ (°), Cu Kα radiation

Figure 5

a)

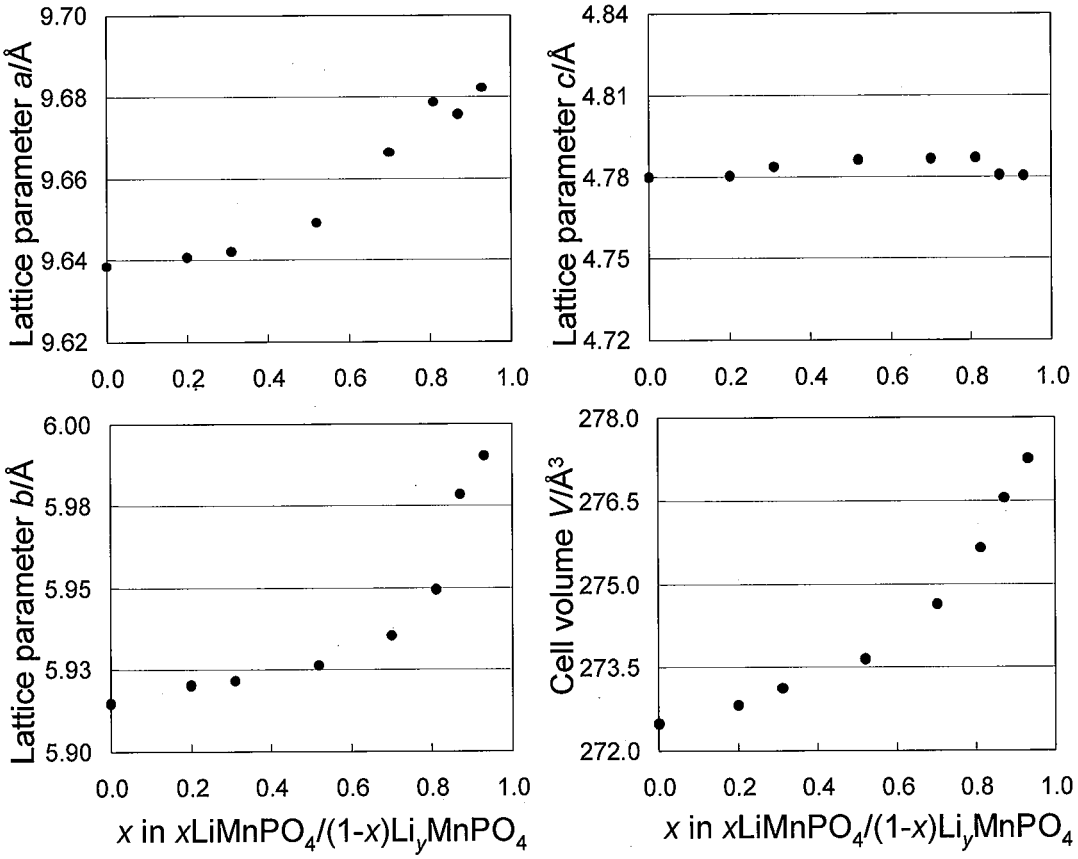
Lattice parameter a/Å
9.70
9.68
9.66
9.64
9.62
Lattice parameter c/Å
4.84
4.81
4.78
4.75
4.72
Lattice parameter b/Å
6.00
5.98
5.95
5.93
5.90
Cell volume V/Å3
278.0
276.5
275.0
273.5
272.0
0.0
0.2
0.4
0.6
0.8
1.0
x in xLiMnPO4/(1-x)LiyMnPO4
x in xLiMnPO4/(1-x)LiyMnPO4

b)

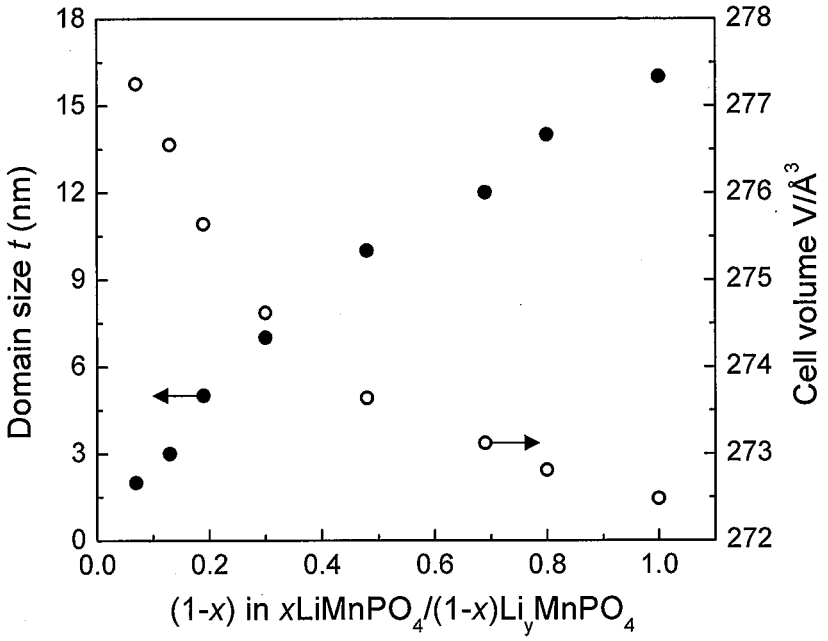
Domain size t (nm)
Cell volume V/Å3
(1-x) in xLiMnPO4/(1-x)LiyMnPO4
0
3
6
9
12
15
18
272
273
274
275
276
277
278
0.0
0.2
0.4
0.6
0.8
1.0

c)

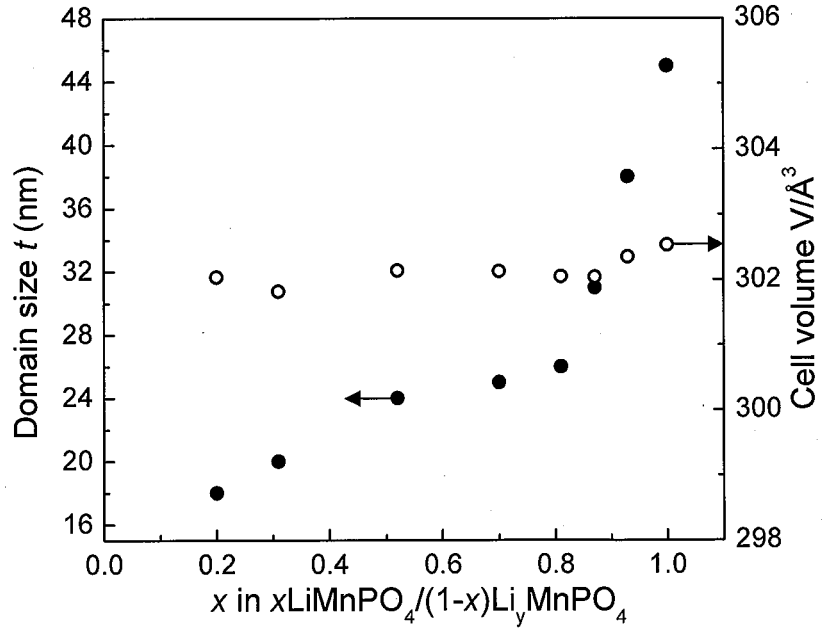
Domain size t (nm)
Cell volume V/Å3
x in xLiMnPO4/(1-x)LiyMnPO4
16
20
24
28
32
36
40
44
48
298
300
302
304
306
0.0
0.2
0.4
0.6
0.8
1.0

Figure 6

a)

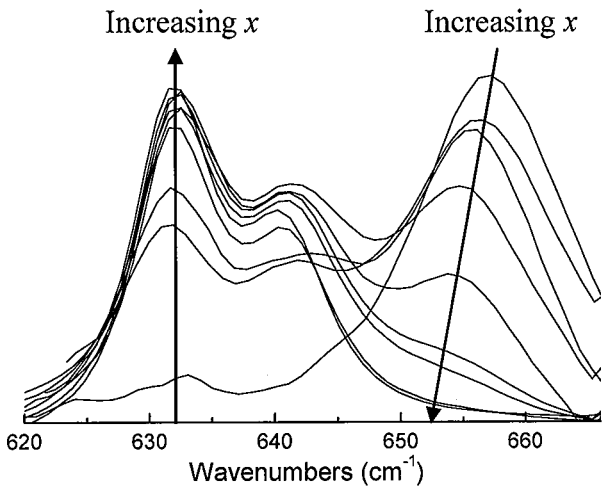
Increasing x
Increasing x
620
630
640
650
660
Wavenumbers (cm^{-1})

b)

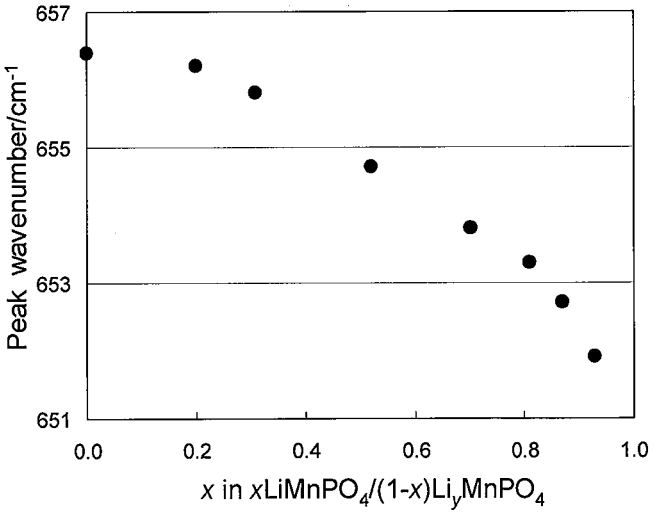
657
655
653
651
Peak wavenumber/cm^{-1}
0.0
0.2
0.4
0.6
0.8
1.0
x in xLiMnPO$_4$/(1-x)Li$_y$MnPO$_4$

Figure 7

a)

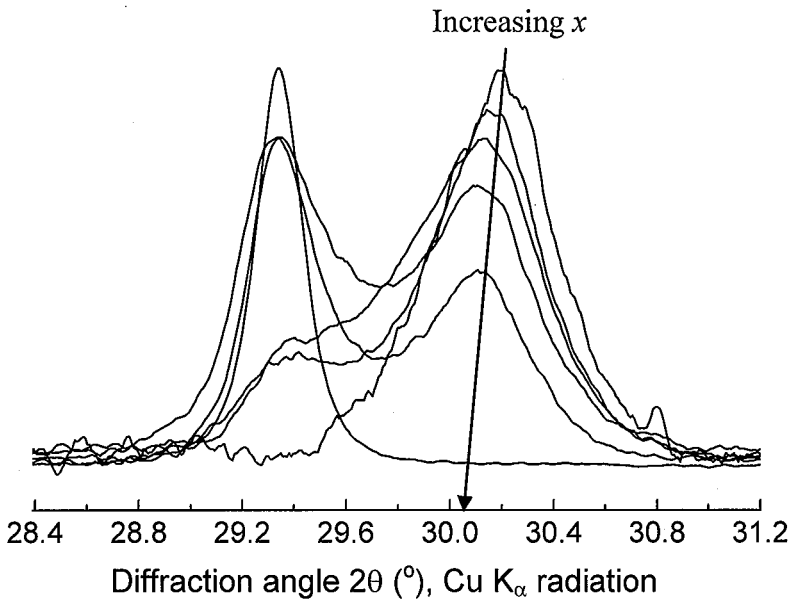
Increasing x
28.4
28.8
29.2
29.6
30.0
30.4
30.8
31.2
Diffraction angle 2θ (°), Cu Kα radiation

b)

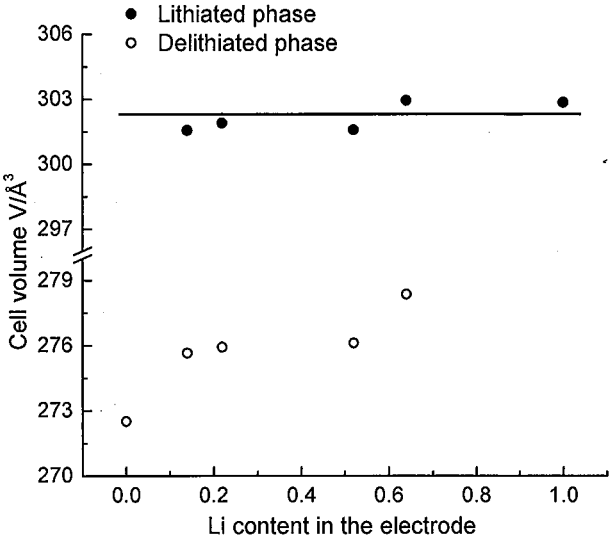
Lithiated phase
Delithiated phase
306
303
300
297
279
276
273
270
Cell volume V/Å3
0.0
0.2
0.4
0.6
0.8
1.0
Li content in the electrode

Figure 8

a)

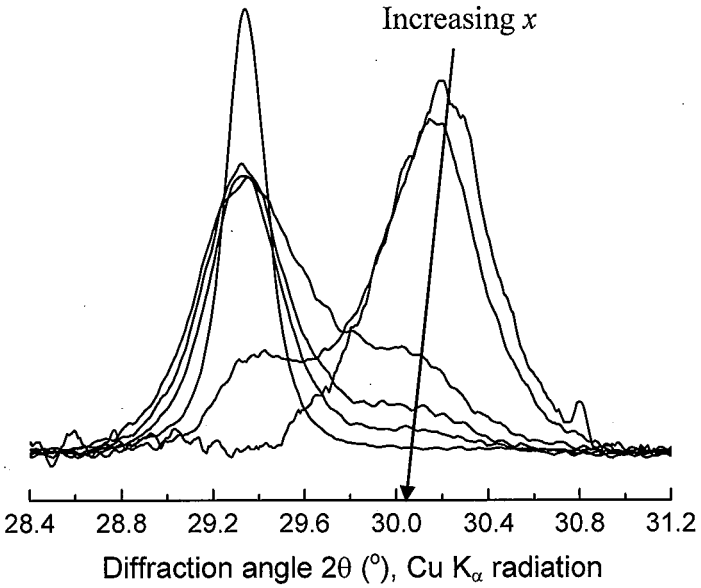
Increasing x
28.4
28.8
29.2
29.6
30.0
30.4
30.8
31.2
Diffraction angle 2θ (°), Cu Kα radiation

b)

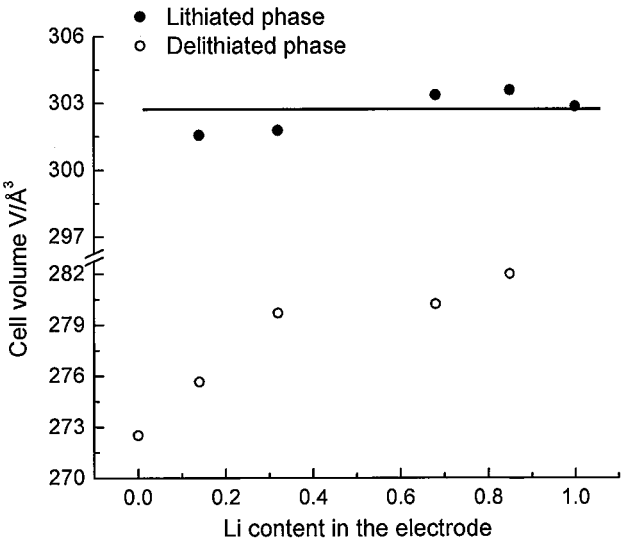
Lithiated phase
Delithiated phase
306
303
300
297
282
279
276
273
270
Cell volume V/Å3
0.0
0.2
0.4
0.6
0.8
1.0
Li content in the electrode

Figure 9

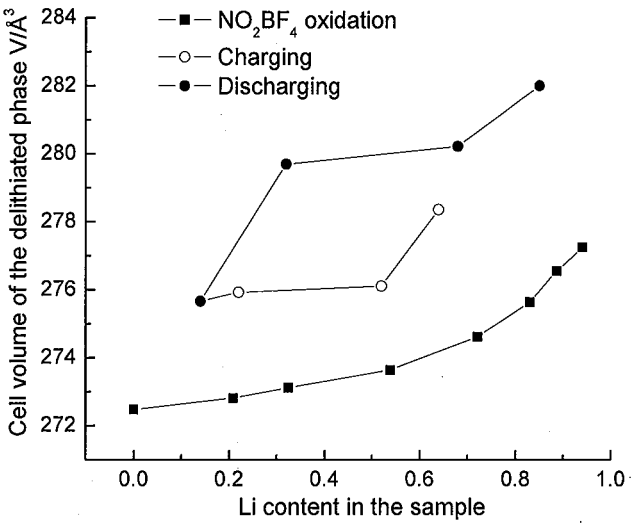
NO2BF4 oxidation
Charging
Discharging
Cell volume of the delithiated phase V/Å3
284
282
280
278
276
274
272
0.0
0.2
0.4
0.6
0.8
1.0
Li content in the sample

Figure 10

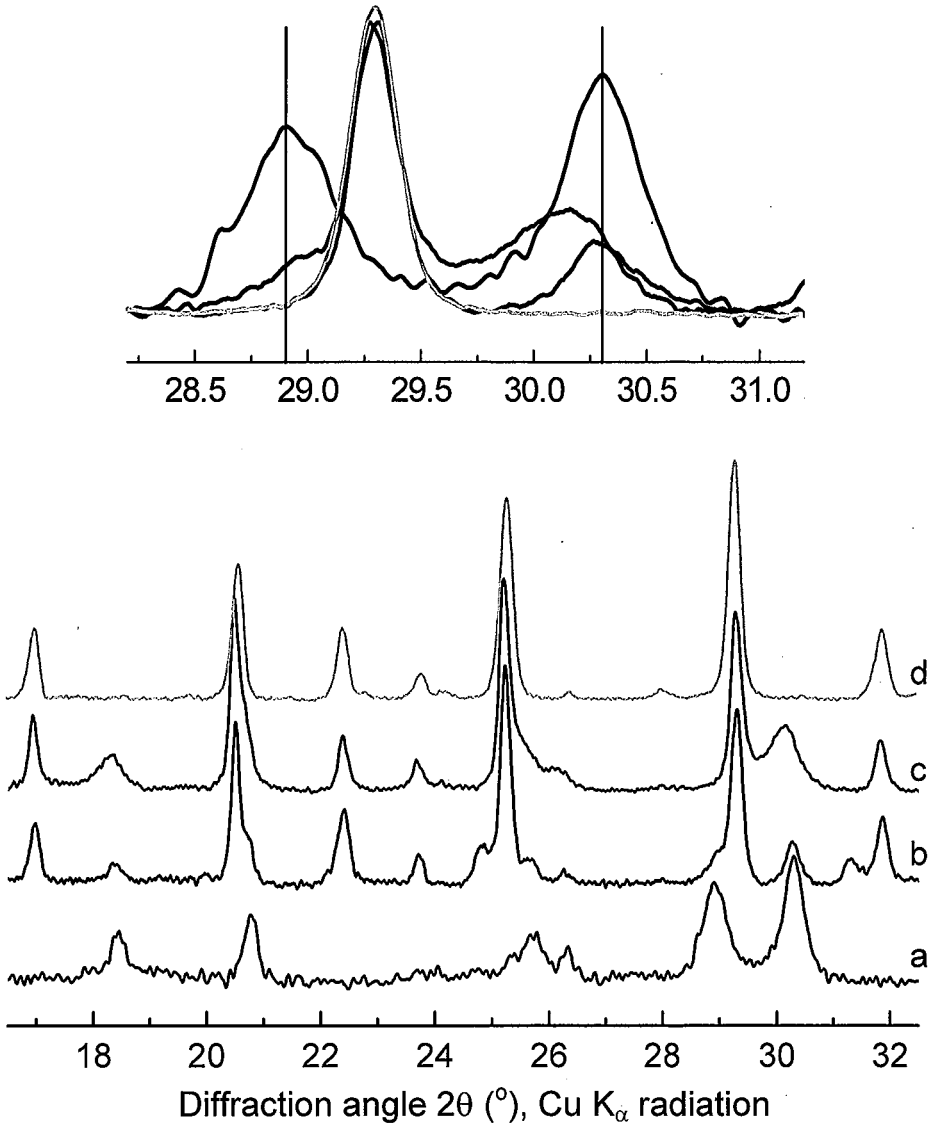
28.5
29.0
29.5
30.0
30.5
31.0
d
c
b
a
18
20
22
24
26
28
30
32
Diffraction angle 2θ (°), Cu Kα radiation

Figure 11